

A Scheme to Classify Clouds with the Depolarization Ratio and Backscattering Coefficient Measured by Lidar

Kengo IOKIBE *, Yoshitaka TOYOTA, Osami WADA and Ryuji KOGA

Graduate School of Natural Science and Technology, Okayama University
3-1-1 Tsushima-naka, Okayama 700-8530, Japan

(Received January 12, 2005)

The optical properties of clouds were measured with a polarization Mie lidar during April, 2004 and investigated to categorize the particles detected by the lidar. The cloud layers were categorized into five types according to the depolarization ratios, as follows: (I) constant and small (less than 5%); increasing with height (II) nearly from 0% and (III) from about 50%; (IV) large and varying with the backscattering coefficient; and (V) sharply decreasing. This categorization of clouds enabled us to separate aerosols from clouds in a lidar signal. Comparison of the backscattering coefficients between clouds of types (I) and (II) suggested that the depolarization ratio induced by multiple scattering in dense clouds does not depend on the particle density. Estimation of the particle phase for the five cloud categories was also examined.

1 INTRODUCTION

A ground-based polarization Mie lidar has been installed at Okayama University. It can automatically and successfully measure aerosol optical properties, viz. the backscattering and extinction coefficients and the depolarization ratio, in the troposphere. This lidar has also successfully obtained height profiles of such properties in long-term measurement projects.[1] The signal received by the lidar contains information related to the optical properties of aerosol and cloud particles, including mineral dust, ash, chemical pollutants like sulfates, and liquid- and ice-cloud particles. To extract the aerosol characteristics from a lidar signal that includes echoes from both aerosols and clouds, it is necessary to separate the aerosol and cloud components in the signal. We previously devised an empirical framework for using the range-

corrected signal intensity and depolarization ratio to determine the particle type dominating a detected layer.[1] This framework, however, was incomplete in two respects—an inadequate number of cloud categories, and an arbitrary unit for the range-corrected signal intensity. Clouds were categorized into only two types, water and ice clouds, delineated by a depolarization ratio of 20%. The depolarization ratio in a cloud layer, however, involves the multiple scattering effect and reportedly ranges from 10 to 50% in ice clouds,[2, 3] so more detailed classification is required. In addition, though the signal intensity is a convenient measure indicating the relative distributions of particle densities, these relative quantities are inadequate for establishing a cloud-classification scheme. Instead, such a scheme requires statistical analysis in which the quantitative properties of clouds, obtained from large amounts of lidar data, should be investigated.

In this paper, we categorize clouds in terms of the height distribution of the depolarization ratio. An

*E-mail iokibe@dev.cne.okayama-u.ac.jp

alternative measure, the particle backscattering coefficient, is also considered here. The particle backscattering coefficient is an absolute quantity, with the dimension of $[\text{m}^{-1}\text{sr}^{-1}]$, that represents the scattering rate in terms of the ratio of the backscattered power to the incident power per unit length in the light path and per unit solid angle. Although the backscattering coefficient is difficult to retrieve from a lidar signal, because it contains inherently unknown parameters, we calculate it from some suitable lidar signals for which a matching algorithm using a molecular model[4] estimates one of the unknown parameters, the inversion boundary value, with reasonable accuracy. We then analyze the backscattering coefficients retrieved from signals suitable for this matching method.

2 METHOD

We analyzed echoes from clouds by using a selected lidar signal suitable for an algorithm to estimate the inversion boundary conditions. The backscattering coefficients and depolarization ratios were retrieved from the signals with the well-known methods described below.

2.1 Polarized Mie Lidar

A polarized Mie lidar installed in Okayama, Japan was employed to measure the properties of tropospheric aerosols. The lidar transmits a linearly polarized laser pulse with a wavelength of 532 nm, excited by a Nd:YAG laser, vertically into the atmosphere; it then receives the resultant backscattering from aerosols, clouds, and molecules. The receiver has a polarizing beam splitter that divides the backscattering into two components, parallel and perpendicular to the transmitted polarization. Two photomultipliers are installed for detecting each component individually. The lidar measures the backscattered intensity, which contains information on atmospheric optical properties, including the depolarization ratio, indicating the non-sphericity of aerosol particles.

The lidar is automatically controlled by a lidar operating system (LiOS)[1] according to a fixed schedule of measurement periods starting at 0, 15, 30, or 45 minutes in every hour and ending after seven minutes. During each period, the lidar profiles are averaged for 4096 laser pulses.

2.2 Analysis of Echoes from Clouds

The methods of retrieving the particle backscattering coefficient and the depolarization ratio from a lidar signal are described here.

Particle backscattering coefficient

The height distributions of the particle (aerosol) backscattering coefficient were calculated from a lidar profile by using the inversion method given by Fernald.[5,6] This method gives the backscattering profile as

$$\beta_A(z) + \beta_M(z) = \frac{X(z)C(z)}{\frac{X(z_c)}{\beta_A(z_c) + \beta_M(z_c)} + 2S_A \int_z^{z_c} X(z')C(z')dz'}, \quad (1)$$

$$C(z) = \exp \left[2(S_A - S_M) \int_z^{z_c} \beta_M(z')dz' \right],$$

where $\beta(z)$ and $X(z)$ represent the backscattering coefficient and the range-corrected lidar return from altitude z , respectively; the S parameters are the lidar ratios, and z_c is the boundary altitude. The subscripts A and M stand for aerosol and molecule, respectively. Retrieving β_A required assumptions about three of the variables in Eq. (1), namely, $\beta_A(z_c)$, S_A , and β_M , because the height distributions of aerosol and molecule properties, including the size, shape, and phase, on the lidar path change momentarily. The other variables, $X(z)$ and S_M , were known in advance. The former was directly measured, while the latter was theoretically determined as $S_M = 8\pi/3$. [7]

The three unknowns in Eq. (1) were treated as follows. The boundary value was given as $\beta_A(z_c) = 0$ $[\text{m}^{-1}\text{sr}^{-1}]$ at an altitude z_c where the atmosphere was deemed aerosol-free from the results of lidar signal matching to a molecular profile based on the molecular model noted above,[4] which also gives $\beta_M(z)$. The aerosol lidar ratio S_A was fixed at a constant value of 30 sr for ease of calculation, although it usually ranges from 10 to 100 sr, depending on the aerosol composition of the atmosphere.

Not all of the lidar returns were developed into valid aerosol backscattering profiles, because the matching to a molecular profile sometimes found no aerosol-free area over the lidar path. The matching failed founding this case, or when the signal-to-noise ratio of the received signal was very low in the aerosol-free area.

Depolarization ratio

The depolarization ratio, δ , is the ratio of the perpendicular and parallel polarization components in backscattered light. It is given by

$$\delta(z) = \frac{P_{\perp}(z)}{P_{\parallel}(z)}, \quad (2)$$

where P_{\parallel} and P_{\perp} are the received powers of the backscattered light with linear polarization parallel

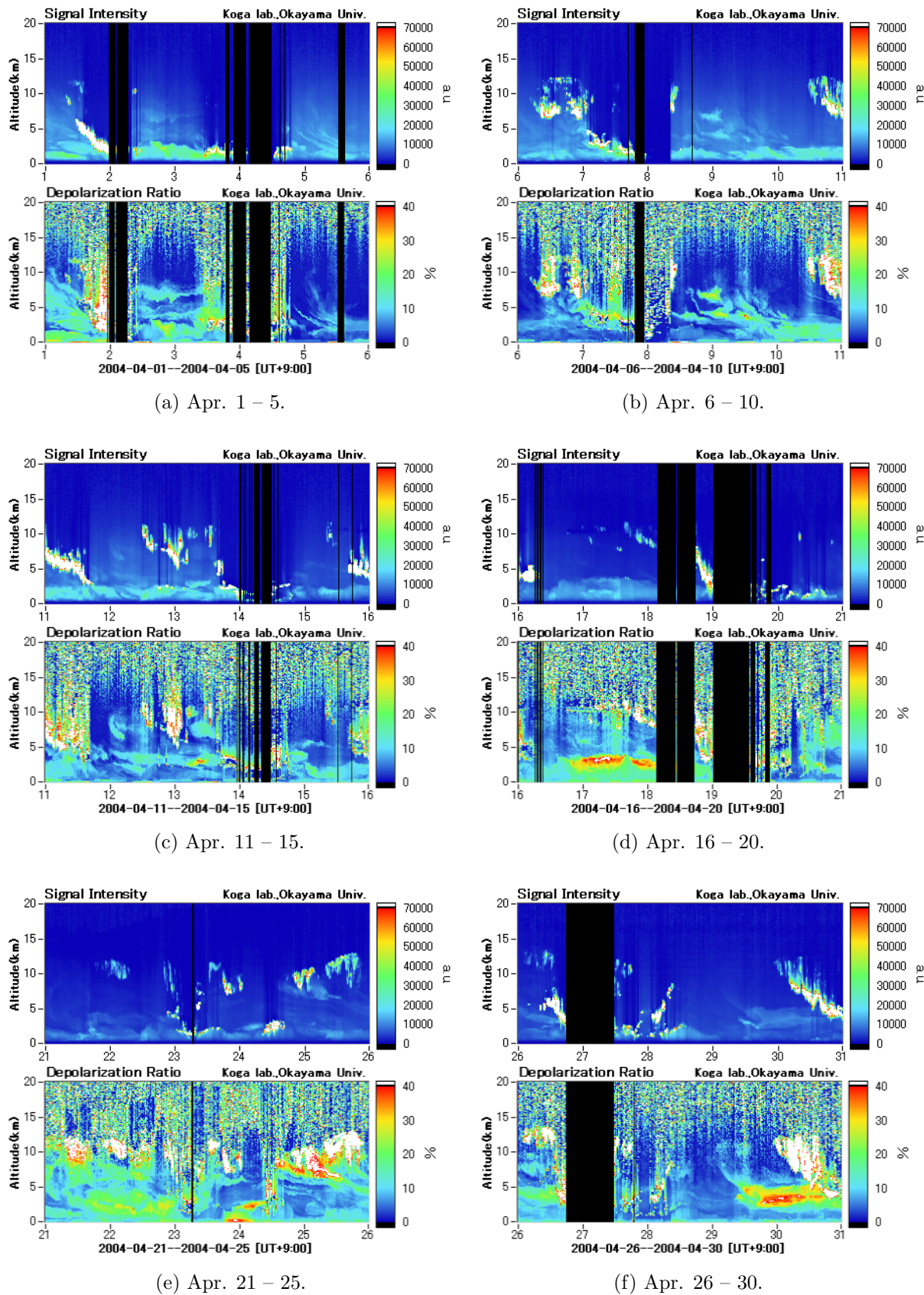


Figure 1: Measured height profiles of range-corrected backscattering intensity and depolarization ratio in Apr. 2004.

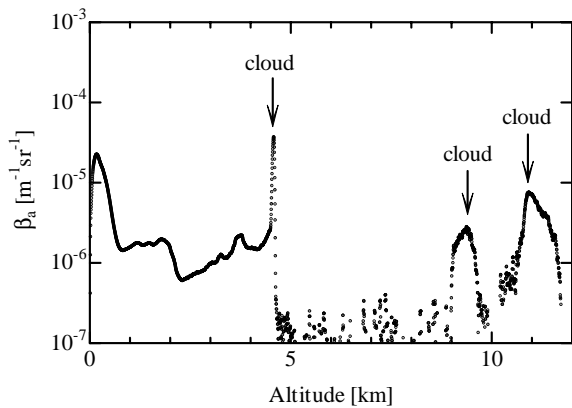


Figure 2: An analyzed backscattering profile including cloud layers, indicated by sharp peaks at $z = 4.6$, 9.4 , and 11.0 km.

and perpendicular, respectively, to the polarization of the transmitted light. The depolarization ratio is a measure of the non-sphericity of aerosol and cloud particles. Spherical particles like water droplets cause no depolarization, so that $\delta = 0$, whereas non-spherical particles, such as ice clouds and mineral dusts, do produce depolarization, so that $\delta > 0$.

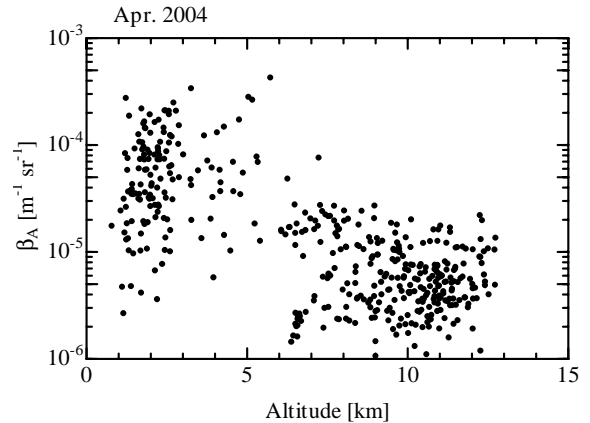
2.3 Data Set

The height profiles of the particle backscattering coefficient and the depolarization ratio obtained in Apr. 2004 were analyzed in order to characterize the clouds in which the measurements took place. Figure 1 shows all of the height profiles of the range-corrected backscattering intensity and the depolarization ratio measured successively during that month.

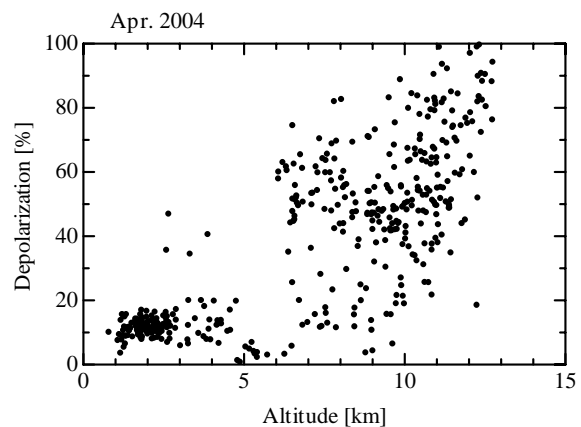
The backscattering coefficient and the depolarization ratio could be read from each height profile at the height where the backscattering profile has a sharp local maximum. The pair of values was then considered representative of the layer containing the sharp peak. The layer was estimated as a cloud layer according to the empirical knowledge that cloud layers have apparent peaks in the height profiles of range-corrected signal intensities and backscattering coefficients. Figure 2 shows an example of an aerosol backscattering profile that includes three apparent cloud peaks at $z = 4.6$, 9.4 , and 11.0 km.

3 RESULTS AND DISCUSSION

Figure 3 shows the height distributions of (a) the particle backscattering coefficient β_A and (b) the depolarization ratio δ as representative quantities for



(a) Particle backscattering coefficient



(b) Depolarization ratio

Figure 3: Height profiles of the (a) backscattering coefficient and (b) depolarization ratio extracted from cloud layers in the lidar profiles measured in Apr. 2004.

cloud layers from the lidar records obtained in Apr., 2004. The plots below and above the altitude of 6 km indicate different features with respect to each other. Larger backscattering coefficients of up to $5 \times 10^{-4} \text{ m}^{-1} \text{ sr}^{-1}$ were measured below 6 km, while smaller coefficients of up to $8 \times 10^{-5} \text{ m}^{-1} \text{ sr}^{-1}$ were measured in the upper range. On the other hand, larger depolarization ratios of up to 100% or more were measured in the upper range, while smaller ratios, almost all less than 20%, were measured in the lower region. These results indicate two cloud trends. The first is that the densities of cloud particles are greater at lower altitudes than at upper altitudes. The second is that the shapes of cloud particles are likely to be spherical at lower altitudes, while they seem non-spherical in the upper range, where temperatures are low enough for water droplets to freeze.

In these graphs, most of the plots are found in the ranges below 3 km and above 6 km. In Fig. 1, on the other hand, intense echoes from clouds are also seen in the height range from 3 to 6 km. This contradiction suggests the likelihood of the matching method failing to find the aerosol-free area in a lidar profile involving echoes from dense clouds, which cause aerosol-free areas to appear absent in the range where they exist. In addition, these dense clouds degrade the SNR in the lidar signal above the range, because they severely defuse the laser beam. These clouds-induced effects reduced the number of plots obtained in the range from 3 to 6 km, as shown in Fig. 1.

Clouds below 6 km

The depolarization ratios increase with height in the cloud layers indicated by the arrows in Fig. 4, and they decrease above the heights where β_A exhibits peaks. The depolarization increase with penetration depth into clouds has been estimated previously.[8–11] It is induced by multiple scattering of the lidar beam in dense water clouds. The increase in δ occurs in the range of β_A from 10^{-6} to $3.2 \times 10^{-3} \text{ m}^{-1}\text{sr}^{-1}$.

Constant depolarization profiles were also found inside the cloud layers shown in Fig. 5. All through the layer shown in Fig. 5(a), a δ value of less than 5% was retained. According to the Mie theory, small δ is produced by spherical particles, so the cloud layer must have been occupied by such particles. The constant distribution of δ indicates the absence of multiple scattering in the layer, although the peak of β_A was $5.4 \times 10^{-5} \text{ m}^{-1}\text{sr}^{-1}$, comparable to the β_A peak of $4.1 \times 10^{-5} \text{ m}^{-1}\text{sr}^{-1}$ in the layer from 1.9 to 2.2 km shown in Fig. 4(a), in which δ , in contrast, increases with height. Another layer, shown in Fig. 5(b), also had small δ of about 5% between 4.9 and 5.4 km, while δ grew to 14% near the cloud bottom. The layer should have developed a depolarization increase, like the layers shown in Fig. 4, assuming it caused multiple scattering of the laser beam. The layer shown in Fig. 5(b) is thus considered to have a different quality from those shown in Fig. 4 and instead related to the particle sphericity, like the layer shown in Fig. 5(a). In addition, a constant depolarization ratio is also seen in the layer between 2.4 and 2.7 km in Fig. 4(a).

The cloud layer shown in Fig. 6 involves a δ distribution differentiated from those in the former cases. The depolarization in this case grew to 30% with the increase in β_A near the bottom; it then varied with a complicated profile and reached 80% at the top. Since these behaviors were also exhibited by higher clouds, as described below, this layer was likely composed of non-spherical ice particles.

Clouds above 6 km

Higher clouds, above an altitude of 6 km, can be divided into four categories based on their depolarization ratio profiles. Depolarization ratios increasing with penetration from about 50% at the cloud bottoms were measured as shown in Fig. 7. Such large depolarization ratios indicate that the clouds were composed of non-spherical ice particles. The ratios continue to increase all through a layer even when β_A decreases, as in the case of the increasing depolarization ratio inside lower clouds shown in Fig. 4. The gradients of the increases in these upper clouds, however, were more gradual than those in the lower clouds (note that the horizontal and vertical scales in the two figures are both different). This difference in gradients agrees with the results of Monte Carlo simulations[11,12] showing that the multiple scattering depolarization is less significant for non-spherical particles than for spherical ones. The larger gradient in Fig. 7(c), as compared to the others, may be attributable to the particle size, according to a simulation result indicating that smaller particles in ice clouds cause a higher multiple-scattering-induced depolarization ratio as compared to larger particles.[11]

Small, constant depolarization ratios were also measured in upper altitudes above 6 km and almost up to 9 km, as shown in Fig. 8, where it must have been enough cold to freeze water droplets. Since the small δ is indicative of water clouds, the cloud layers might have consisted of supercooled water droplets.

In Fig. 9, δ varies with β_A in the cloud layers. Here, the depolarization ratios grow with the penetration depth into clouds, as in the cases shown in Fig. 4 and 7, but they begin to decrease with decreasing β_A . It was previously reported that the depolarization ratio in contrail-cirrus clouds range from about 10 to 50% with different shapes of ice crystals[2] and from 30 to 70 % with temperatures ranging from -60° to -50°C . [3] The height distribution of the depolarization ratio can thus be connected to the shapes of crystals or the temperatures in clouds. The simultaneous changes in the depolarization ratio and the backscattering coefficient suggest dependence of the ratio on the size and/or density of cloud particles.

The clouds shown in Fig. 10 exhibit sharp declines in the depolarization ratio inside the layers. The declines occur at altitudes where β_A increases with a different slope from that at lower altitudes. This may indicate that the cloud phase changed at that altitude from an iced, non-spherical phase with large δ to a phase with small δ or to a mixed (iced non-spherical and liquid spherical) phase.

Classification of clouds

By examining the height distributions of the cloud

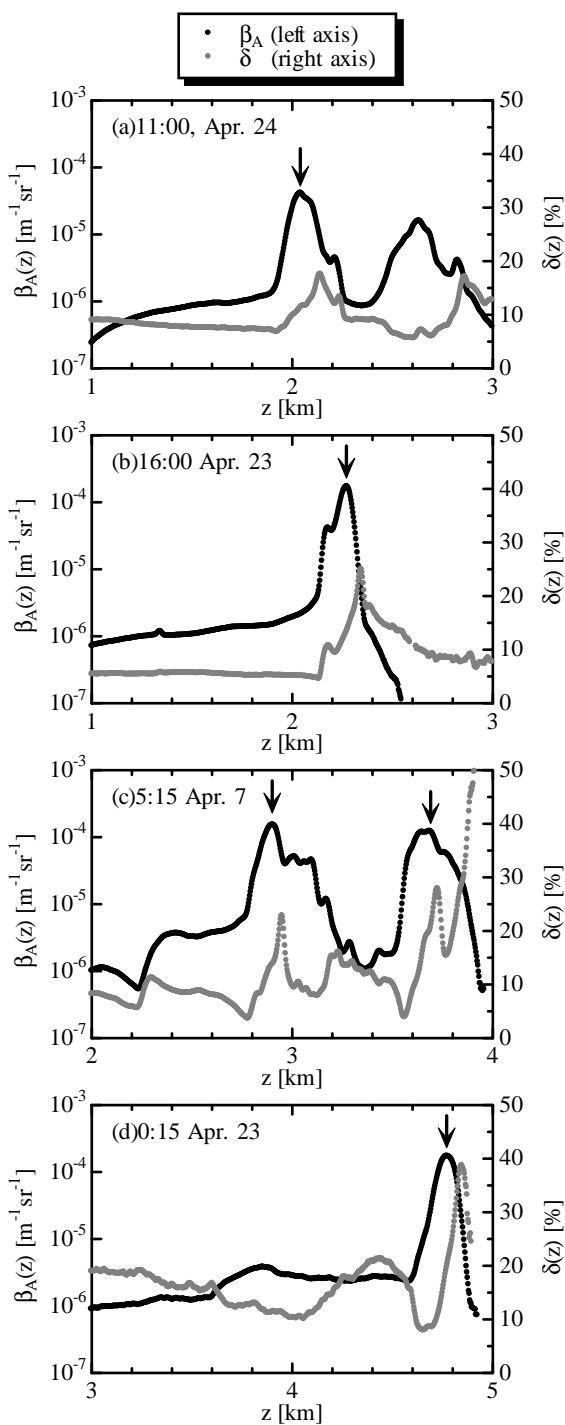


Figure 4: Height distributions of the depolarization ratio δ (right vertical axis) and the particle backscattering coefficient β_A (left vertical axis). The ratios increased over the cloud layers indicated by the arrows and began to decrease at a height where β_A was already decreasing.

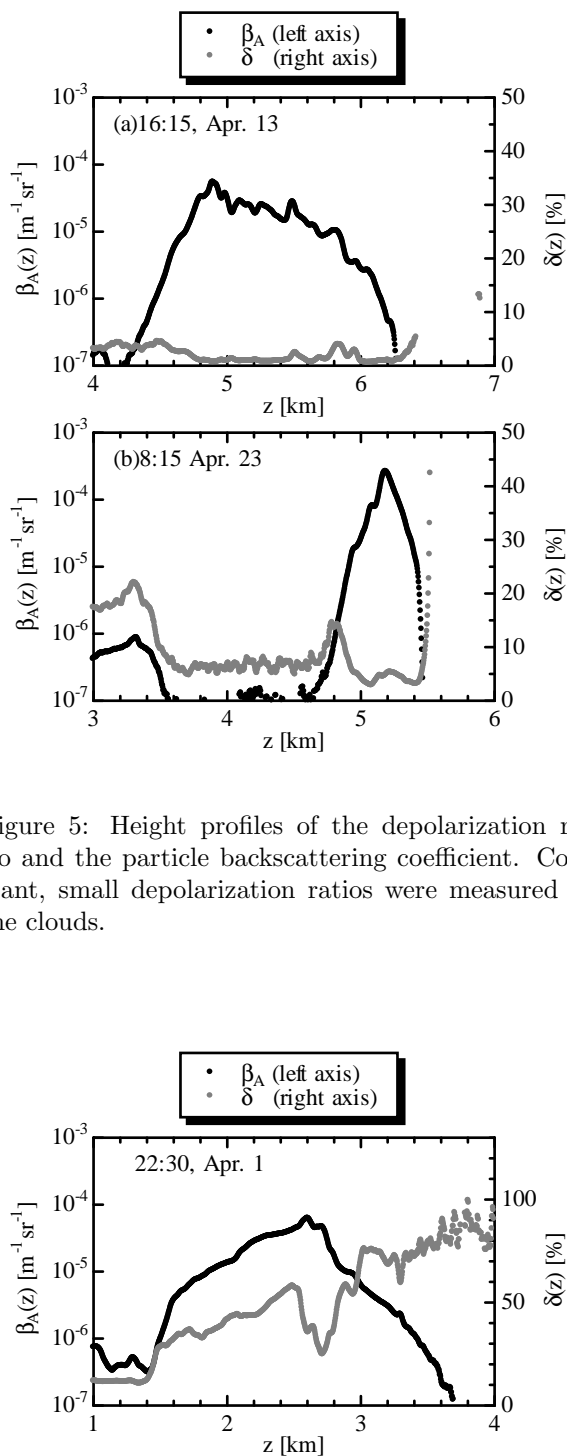


Figure 5: Height profiles of the depolarization ratio and the particle backscattering coefficient. Constant, small depolarization ratios were measured in the clouds.

Figure 6: Height distributions of the depolarization ratio and the particle backscattering coefficient. The depolarization varied with a complicated profile with no apparent relation to that of the backscattering coefficient.

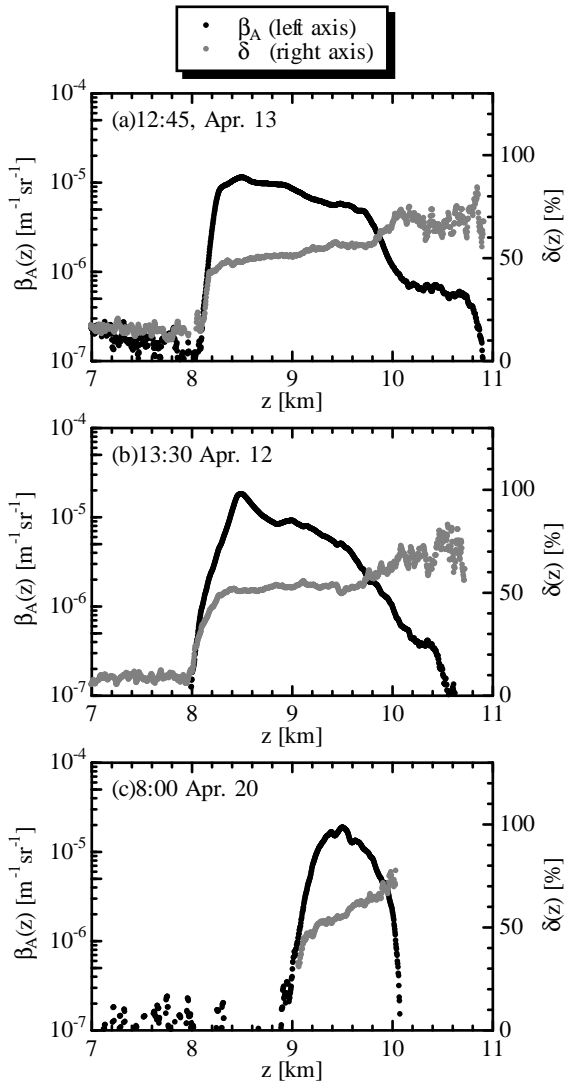


Figure 7: Height distributions of the depolarization ratio and the particle backscattering coefficient. The depolarization ratios increased from about 50% with the penetration depth.

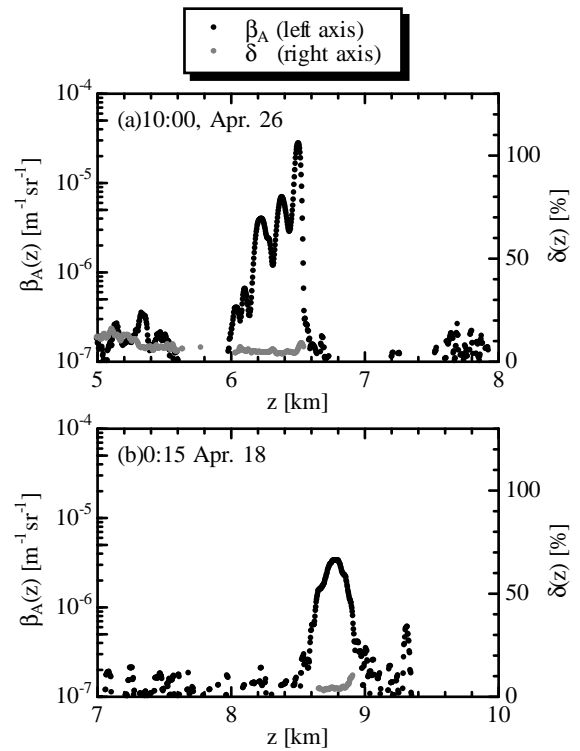


Figure 8: Height distributions of the depolarization ratio and the particle backscattering coefficient. Small depolarization ratios continued from the bottoms to the tops of the clouds.

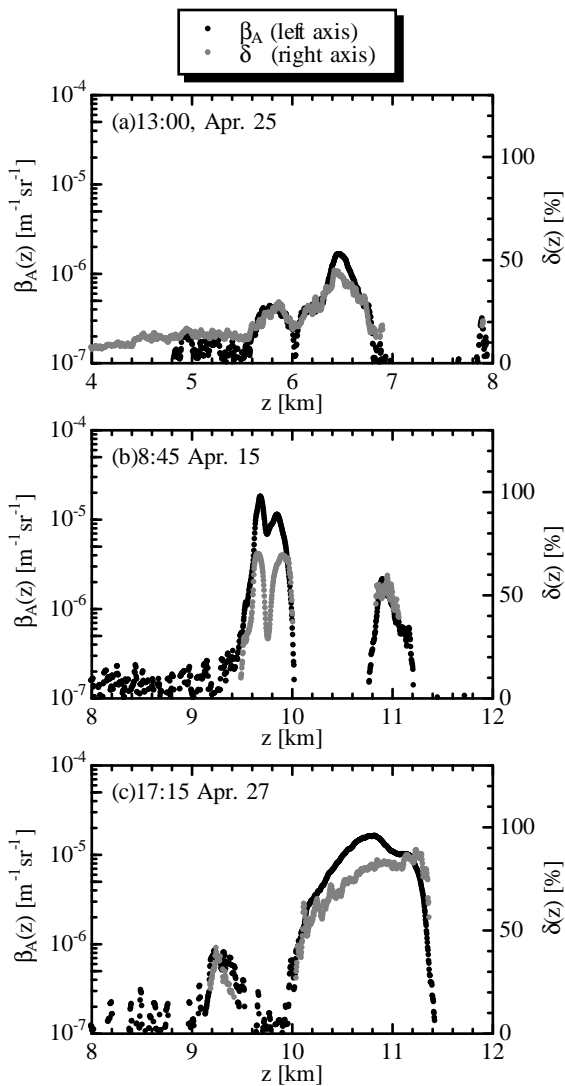


Figure 9: Height distributions of the depolarization ratio and the particle backscattering coefficient. The depolarization ratios changed simultaneously with the backscattering coefficients.

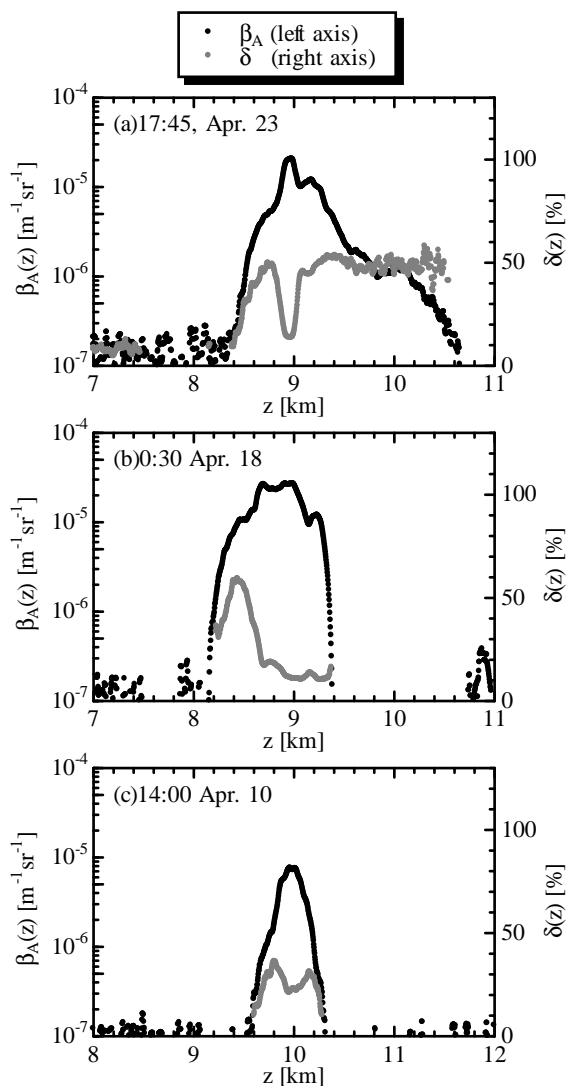


Figure 10: Height distributions of the depolarization ratio and the particle backscattering coefficient. The cloud layers contained sharp declines in the depolarization ratio.

Table 1: Cloud categories.

Type	Height distribution of δ .
I	Constant and small ($\delta \sim 0$).
II	Increasing with penetration depth from $\delta \simeq 0\%$.
III	Increasing with penetration depth from $\delta \simeq 50\%$.
IV	Following the variation of β_A .
V	Sudden decrease to 10-20% between large- δ layers.

depolarization ratios shown in Figs. 4 to 10, we could categorize the clouds according to the depolarization ratio. The cloud layers in the seven cases can be divided into five categories, as shown in Table 1. Clouds with constant small depolarization ratios, as shown in both Fig. 5 and Fig. 8, are categorized into category II. The case of Fig. 6, involving an intricate depolarization ratio distribution, belongs to three categories, III, IV, and V.

This classification is based simply on the height distribution of the lidar depolarization ratio, rather than on the physical or meteorological properties (i.e., the size, phase, shape, temperature, and cloud type) of the clouds. By classifying clouds according to these categories, we can count the frequency of appearance for each category.

4 CONCLUSIONS

The backscattering coefficient and depolarization ratio profiles measured with a polarization Mie lidar were analyzed to categorize cloud types. Our analysis concluded that cloud layers can be categorized into five types according to the height profile of the depolarization ratio in the cloud layers. This classification can thus be used to determine cloud layers from a lidar signal.

The classification scheme distinguishes clouds according to the features of the lidar depolarization ratio in cloud layers, rather than the physical properties (phase, size, shape, and temperature) of clouds. Further statistical studies with larger numbers of samples could be applied to identify the physical properties for the categories in this scheme. In spite of the discussion above, the mechanism producing differences in the depolarization variation between two categories of dense clouds is unclear. Comparable backscattering coefficients in different cloud types suggest that the depolarization induced by multiple scattering does

not depend on the cloud density.

References

- [1] K. Iokibe, Y. Toyota, O. Wada, and R. Koga: *Memoirs Faculty of Eng. Okayama Univ.*, **37-2** (2003), 89–97.
- [2] V. Freudenthaler, F. Homburg, and H. Jäger: *Geophys. Res. Lett.*, **23** (1996), 3715–3718.
- [3] K. Sassen and C.-Y. Hsueh: *Geophys. Res. Lett.*, **25** (1998), 1165–1168.
- [4] NASA: 1976 U. S. Standard Atmosphere Supplement: U. S. GPO, Washinton D. C., 1976.
- [5] F. G. Fernald, B. M., and J. A. Reagan: *J. Appl. Meteor.*, **11** (1972), 482–489.
- [6] F. G. Fernald: *Appl. Opt.*, **23** (1984), 652–653.
- [7] E. D. Hinkley, Ed.: *Laser Monitoring of the Atmosphere*, chapter 4: Springer-Verlag, New York, 1976.
- [8] S. R. Pal and A. I. Carswell: *Appl. Opt.*, **12** (1973), 1530–1535.
- [9] K. Sassen and R. L. Petrilla: *Appl. Opt.*, **25** (1986), 1450–1459.
- [10] Y.-Y. Sun and Z.-P. Li: *Appl. Opt.*, **28** (1989), 3633–3638.
- [11] Y.-X. Hu, D. Winker, P. Yang, B. Baum, L. Poole, and L. Vann: *J. Quant. Spectrosc. Radiat. Transf.*, **70** (2001), 569–579.
- [12] Y.-Y. Sun, Z.-P. Li, and J. Bösenberg: *Appl. Opt.*, **28** (1989), 3625–3632.